JCTC Journal of Chemical Theory and Computation

Article

pubs.acs.org/JCTC

# Combining a Dissociative Water Model with a Hybrid QM/MM Approach—A Simulation Strategy for the Study of Proton Transfer Reactions in Solution

Thomas S. Hofer,* Manuel Hitzenberger, and Bernhard R. Randolf

Theoretical Chemistry Division, Institute of General, Inorganic and Theoretical Chemistry, University of Innsbruck, Innrain 80-82, A-6020 Innsbruck, Austria

**ABSTRACT:** An implementation strategy for a dissociative water potential in hybrid QM/MM simulations is outlined. As the knowledge of the time-dependent topology is crucial for the assignment of solvent molecules to the QM or MM subregion, proton transfer events and the associated change of the molecular composition have to be monitored as the simulation is progressing. A simple and effective update criterion is proposed, which was found to be an efficient tool to identify sustained proton transfer reactions. The resulting topology data enable the application of the dissociative solvent model in QM/MM simulations and serve as a reference for the analysis of time-dependent properties such as the proton hopping rate and the diffusion coefficient. For the latter, an interpolation scheme is proposed linking subsequent proton transfer events into a single diffusive entity. Suitable settings of key parameters for the topology update and the interpolation scheme have been determined by analyzing MD trajectories of an excess proton in water and 1 M HCl. The resulting values for the proton hopping rate and the diffusion coefficient are well within the range estimated by EVB models and CPMD approaches. An investigation of the hydrolytic conversion of As(III) to $[As(OH)_2]^+$ serves as an exemplary application of the dissociative model in a QM/MM simulation study.

## 1. INTRODUCTION

During the past decades, the capabilities of computational methods for the treatment of chemical systems have significantly improved. This is particularly true for the computational treatment of liquid systems, which are considered to be the most important but also the most challenging state of matter in chemistry[1−3] (among the relevant states for chemistry being solid, liquid, and gas). In order to successfully perform chemical simulations, an accurate description of the potential energy surface is required, which can be achieved by empirical models[4,5] or via quantum chemical methods.[6−8]

The main advantage of the first approach known as molecular mechanics (MM) of force fields (FF) is its computational efficiency, which strongly depends on the considered interaction types[4,5] (e.g., bonding, nonbonding, polarization, many-body effects, etc.). As the development and balancing of a reliable parameter set for chemical systems is a challenging, tedious, and time-consuming task, the applicability, accuracy, and/or transferability of MM models are in many cases limited. A further severe limitation of MM approaches results from the harmonic approximation (cf. Figure 1a)[4,5]—the majority of force fields treat intramolecular interactions such as bonds and angles via a harmonic spring model, which prevents the description of the formation and cleavage of chemical bonds.

Approaches based on quantum mechanics (QM) employ numerical solutions of Schrödinger's equation[9] to obtain a quantitative description of the electronic structure.[6−8] These methods are considered to be more accurate than force fields as polarization, charge-transfer, and many-body effects are automatically taken into account. As no empirical parameters are used, these methods are very general and can be applied to a broad range of chemical systems. The accuracy of QM approaches is in some cases limited, resulting from approximations in the treatment of the correlation of electrons. Furthermore, the extraordinarily high computational effort required to execute QM approaches prevents the application of these methods to describe an entire simulation box as of yet, and a compromise between accuracy and computational demand has to be sought.

In the Car−Parrinello molecular dynamics (CPMD) framework,[10] this balance is achieved by reducing the system size to a critical minimum (typically to the solute and about 30 and 100 water molecules) and the application of approximate quantum chemical schemes such as density functional theory (DFT)[8] at the generalized gradient approximation (GGA) level.[8] Although this approach has become quite popular resulting from the comparably low computational demand, recent data for pure water have revealed a number of method-inherent shortcomings, leading to an inaccurate description of hydrogen-bonded systems. In this framework, the melting point of water was estimated as approximately 410 K,[11] and it was concluded that the description of water at room-temperature shows the characteristics of a supercooled liquid.[12]

An alternative approach exploiting the advantages of quantum mechanical and molecular mechanical methodologies are hybrid QM/MM approaches.[13−18] In this framework, the system is partitioned into two sub-regions. While the

**Special Issue:** Wilfred F. van Gunsteren Festschrift

**Received:** January 29, 2012
**Published:** March 30, 2012

ACS Publications © 2012 American Chemical Society

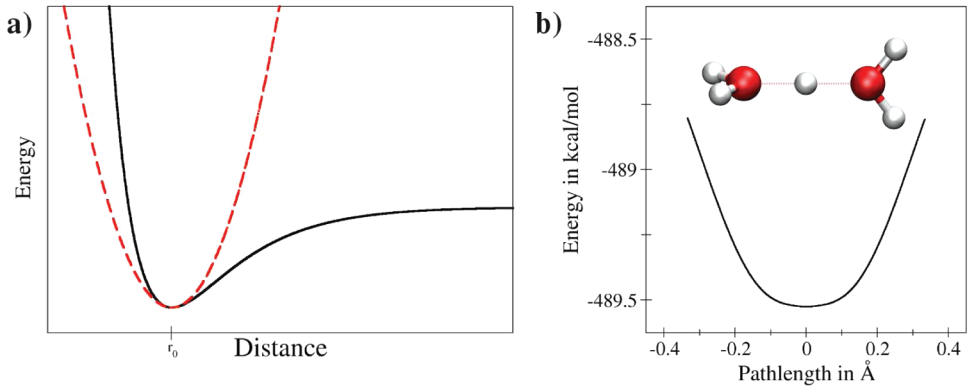


**Figure 1.** (a) The majority of force-fields employ the harmonic approximation (dashed line) to model a chemical bond (solid line). (b) Potential energy profile obtained from eigenvector following in the $H_5O_2^+$ system described by the Garofalini model.

chemically most relevant part is treated via a suitable quantum chemical approach, molecular mechanical potentials are considered to be sufficiently accurate to describe the remaining part of the system. Whereas the computation of energies and forces within the respective sub-regions results from the straightforward application of the associated theoretical method, the coupling of the two zones is challenging, and a large number of different coupling protocols has been developed.[14] As solvent molecules are assigned as a whole to either the QM or the MM region, water molecules are never fragmented by the QM/MM interface.[19,20] To ensure a continuous change of forces upon particle migration to/from the quantum mechanical region, smoothing procedures have been developed,[20−22] gradually shifting the forces from the QM to the MM contribution.

One particularly challenging application for QM/MM simulations is the study of hydrolysis phenomena. Although the quantum chemical treatment is capable of describing proton transfer events occurring within the QM region, the majority of molecular mechanical methods does not enable an adequate treatment of oxonium ($H_3O^+$) and hydroxide ($OH^-$) ions. Simulations have to be aborted as soon as one of the protonated species migrates into the MM region (see for example a QM/MM study of the hydrolytic conversion of As(III) to $H_3AsO_3$[23]). Although it is certainly possible to parametrize the interaction between $H_3O^+$ and the solvent, the inability of MM methods to describe the formation and cleavage of chemical bonds prevents the description of proton transfer events in the MM region, which is a prerequisite for a chemically sound treatment of an excess proton in water. The same applies to hydrolysis events leading to hydroxide ions, as has been observed in the case of the hydrolytic conversion of $AsO_4^{3-}$ to $HAsO_4^{2-}$.[24] The simulation had to be aborted as soon as the $OH^-$ migrated into the MM region.

To overcome this limitation, interaction potentials that do not rely on the harmonic approximation have to be employed, to describe the solvent in the MM region. Already, the central force model for liquid water derived by Stillinger and co-workers[25−27] was in principle capable of describing stable oxonium and hydroxide ions (the parametrization did not consider an application to (de)protonated water molecules, though). A protonizable water model for quantum dynamical simulations was presented by Billeter and van Gunsteren.[28,29] This approach employs monopole−dipole interactions and variable Lennard-Jones functions to describe the proton−protolyte interactions. A widely used methodology to investigate proton transfer reactions employing the valence bond concept of chemical bonding is the multistate empirical valence bond (MS-EVB) approach.[30] In this method, the electronic state for a particular configuration is represented by a superposition of states, which are modeled via empirical potentials. A variety of parametrizations for excess protons are available today,[31−37] and the approach has been extended to model hydroxide ions in solution as well.[38] The functional form of the water potential developed by Mahadevan and Garofalini[39] based on atom-centered pair and three-body contributions enables a straightforward application of this solvent model in the context of QM/MM simulations. This dissociative force field for water, technical challenges associated with the implementation in a QM/MM framework, and an exemplary application of this potential in QM/MM simulations are discussed in this manuscript.

## 2. METHODOLOGY

**2.1. The Dissociative Water Model.** In order to achieve a dissociative description of the solvent, no distinction between intra- and intermolecular contributions is made.[39] The potential functions apply in the same manner to all interactions, irrespective of whether the atoms are part of the same residue (hydroxide, water, oxonium, ...) or not. In order to achieve a reliable representation of the potential energy surface, the resulting expressions are considerably more complex than the functional form of conventional water models.[40] In addition to the partial charge $q$ assigned to the atoms, each particle is surrounded by a Gaussian charge distribution carrying a charge $q^d$ (*i.e.*, diffusive charge) of opposite sign to reduce the overall Coulombic potential at increased distances. Thus, the Coulomb interactions between each pair of particles $i$ and $j$ consist of four contributions

$$U_{\text{Coulomb}} = U_{qq} + U_{q^d q} + U_{qq^d} + U_{q^d q^d} \tag{1}$$

which are given as

$$U_{qq} = \frac{q_i q_j}{\|\mathbf{r}_{ij}\|}\operatorname{erfc}(\kappa\|\mathbf{r}_{ij}\|) \tag{2}$$

$$U_{q^d q} = \frac{q_i^d q_j}{\|\mathbf{r}_{ij}\|}\operatorname{erf}\left(\frac{\|\mathbf{r}_{ij}\|}{\sqrt{2}\zeta_{ij}}\right)\operatorname{erfc}(\kappa\|\mathbf{r}_{ij}\|) \tag{3}$$


dx.doi.org/10.1021/ct300062k | J. Chem. Theory Comput. 2012, 8, 3586−3595

$$U_{qq^d} = \frac{q_i q_j^d}{\|\mathbf{r}_{ij}\|}\mathrm{erf}\left(\frac{\|\mathbf{r}_{ij}\|}{\sqrt{2}\zeta_{ij}}\right)\mathrm{erfc}(\kappa\|\mathbf{r}_{ij}\|) \quad (4)$$

$$U_{q^d q^d} = \frac{q_i^d q_j^d}{\|\mathbf{r}_{ij}\|}\mathrm{erf}\left(\frac{\|\mathbf{r}_{ij}\|}{2\zeta_{ij}}\right)\mathrm{erfc}(\kappa\|\mathbf{r}_{ij}\|) \quad (5)$$

where $q_i$, $q_j$, $q_i^d$, and $q_j^d$ are the charges of the point charge and the Gaussian charge cloud assigned to particles $i$ and $j$, respectively; $\mathbf{r}_{ij}$ is the displacement vector; and the coefficient $\zeta_{ij}$ corresponds to the width of the Gaussian charge clouds. The last factor involving the complementary error function erfc results from the application of the Wolf-summation technique,[41,42] in which the Coulombic interactions are damped to account for the influence of local neutralization in chemical systems. $\kappa$ is the corresponding damping coefficient. The non-Coulombic pair contributions consist of a repulsive and a dispersion interaction defined as

$$U_{\text{non-Coulomb}} = U_{\text{rep}} + U_{\text{disp}} \quad (6)$$

$$U_{\text{rep}} = A_{ij}\frac{2\xi_{ij}}{\|\mathbf{r}_{ij}\|}\mathrm{erfc}\left(\frac{\|\mathbf{r}_{ij}\|}{2\xi_{ij}}\right) \quad (7)$$

$$U_{\text{disp}} = \frac{-B_{ij}}{\|\mathbf{r}_{ij}\|^6} \quad (8)$$

where $A_{ij}$, $B_{ij}$, and $\xi_{ij}$ are the respective potential parameters for the particle pair $i$ and $j$. In addition to pairwise interactions, a screened, cosine-harmonic three-body potential is employed, which is given as

$$U_3(\mathbf{r}_{ij}, \mathbf{r}_{ik}, \theta_{jik}) = \lambda_{jik}\exp\left(\frac{\gamma_{ij}}{\|\mathbf{r}_{ij}\| - r_{ij}^0}\right)\exp\left(\frac{\gamma_{ik}}{\|\mathbf{r}_{ik}\| - r_{ik}^0}\right) \times [\cos(\theta_{jik}) - \cos(\theta_{jik}^0)]^2 \quad (9)$$

where $\lambda_{jik}$ corresponds to the force constant, $\mathbf{r}_{ij}$ and $\mathbf{r}_{ik}$ are the displacement vectors of the particles $j$ and $k$ from a central atom $i$, and $\theta_{jik}$ is the angle defined by the particle triple $j-i-k$. $\theta_{jik}^0$ is the associated equilibrium angle. The exponential screening functions ensure that the potential approaches zero for large particle separations. $r_{ij}^0$ and $r_{ik}^0$ are the cutoff distances; $\gamma_{ij}$ and $\gamma_{ik}$ are the respective screening coefficients. Similar to the case of the pair interactions, the three-body potential is applied to all particle triples within the cutoff—no distinction between inter- and intramolecular contributions is made. This functional form of the three-body potential enables the transfer of a proton from a donor to an acceptor atom. Figure 1b displays the potential energy resulting from the eigenvector following (along the normal mode with the largest component parallel to the O−O distance vector) from the minimum in the $H_5O_2^+$ system. The profile agrees well with the reaction coordinate reported from EVB[33,36] and density functional[43] studies. It can be seen that the potential energy path is continuous, which demonstrates that this model is capable of describing the transfer of a proton between two species.

In addition to the capability of treating water in various protonation states, parameters for $Na^+$ and $Cl^-$ ions have been developed for this model.[44] Thus, it is possible to add hydrogen chloride (HCl) and sodium hydroxide (NaOH) to the system, which can be utilized to change the pH value of the system. For instance, in 1 M HCl (density of 1.016 kg/dm$^3$), the weight-percent of HCl is 3.59%, which corresponds to 17 molecules of HCl per 1000 molecules of water. As the model enables dissociation of HCl, a highly acidic solution can be treated. These considerations apply in a similar way for NaOH. To model a 1 M sodium hydroxide solution, 18 molecules of NaOH per 1000 molecules of water have to be treated. Thus, in addition to the possibility to treat excess protons and hydroxide ions that may cross the QM/MM interface, (de)protonation and hydrolysis of solute species located in the QM region can be induced by employing an acidified or basic simulation system. Although simulations of such systems are in principle also possible in the case of Car−Parrinello molecular dynamic simulations,[10] the considerably smaller system sizes achievable in this approach limits the number of acid or base molecules, which might be insufficient to model water at different pH values.

**2.2. Automated Topology Update.** The application of the dissociative model in the context of a QM/MM simulation is considerably more challenging than in a purely classical simulation. In the latter case, no information on the topology of the system is required to perform the simulation. Oxygen and hydrogen atoms are considered as separate species, and molecules are formed according to the respective interatomic forces. The topology of the system (i.e., which atoms form a molecular species at a given configuration) and all related properties can be analyzed from the trajectory when the simulation is complete.

As solvent molecules are assigned as a whole to either the QM or the MM region in hybrid QM/MM simulations,[19,20] the respective topology information has to be known while the simulation is performed. Otherwise, the fragmentation of the solvent molecules would lead to erratic changes of the charge and spin state of the QM subsystem. These unphysical changes of the electronic system would render the execution of a hybrid QM/MM simulation unfeasible.

To avoid such a situation, a book-keeping of all proton transfer events is required, in order to determine the molecular topology in every step of the simulation. A criterion is required to decide whether a transferring proton is still part of its donor molecule or if it has to be assigned to the acceptor species. This condition should be as general and straightforward as possible so that it can also be applied in the case of simple species, e.g., for a proton transfer between HCl and a $F^-$ ion. Furthermore, it appears practical that the criterion employs only the atomic coordinates at the actual step, as a time-dependent update is not applicable whenever an MD simulation is (re)started or in studies that do not propagate the system via equations of motions as it is the case in Monte Carlo simulations or geometry optimizations. Finally, the criterion should only be triggered by sustained proton transfer events, while short-time fluctuations should not be considered, thus avoiding too frequent topology updates.

A criterion based on the donor-hydrogen ($\mathbf{r}_{\text{DH}}$) and donor−acceptor ($\mathbf{r}_{\text{DA}}$) distances appears to be an intuitive approach to assigning the proton to either the donor or the acceptor. Projection of the donor-hydrogen vector onto the donor−

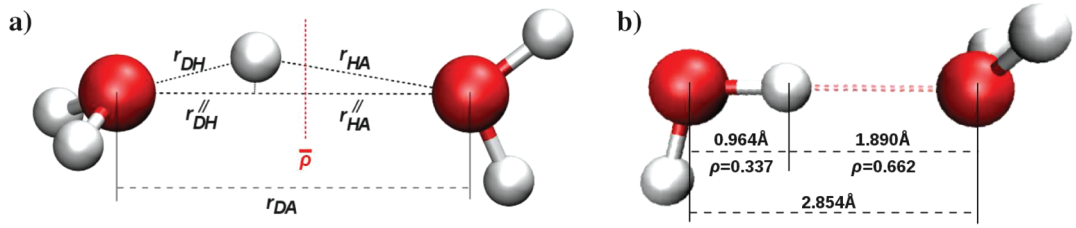


**Figure 2.** (a) Update criterion to monitor proton migration: If the ratio $\rho$ of the projected donor-hydrogen and the donor−acceptor distance vectors $\mathbf{r}_{DH}^{\parallel}$ and $\mathbf{r}_{DA}$ exceeds the threshold $\bar{\rho}$, the proton is assigned to the acceptor species. (b) Minimum configuration of a water dimer optimized in implicit solvent at the CCSD/cc-pVTZ level. In this hydrogen bond, the hydrogen-acceptor ratio amounts to 0.66.

acceptor vector yields the respective parallel component $\mathbf{r}_{DH}^{\parallel}$ (*cf* Figure 2a)

$$\mathbf{r}_{DH}^{\parallel} = \frac{(\mathbf{r}_{DH}^{T}\mathbf{r}_{DA})\mathbf{r}_{DA}}{\|\mathbf{r}_{DA}\|^2} \tag{10}$$

where the superscript T refers to the transpose vector. The use of vector projections for the characterization of hydrogen bonds has been used in the literature before. For instance, an investigation of the quantum nature of hydrogen bonds by Michaelides et al. employed the projected donor−acceptor vectors to characterize the hydrogen bond strength of various chemical compounds.[45]

Next, the ratio $\rho$ of the projected donor-hydrogen bond length and the donor−acceptor distance is determined:

$$\rho = \frac{\|\mathbf{r}_{DH}^{\parallel}\|}{\|\mathbf{r}_{DA}\|} \tag{11}$$

Whenever, this ratio exceeds a threshold value $\bar{\rho}$, the hydrogen is assigned to the acceptor molecule (*c.f.* Figure 2a). It should be noted that although the resulting change of the topology is discontinuous, the underlying potential energy surface remains continuous, thus ensuring a smooth transition of the migrating proton.

The methodology can be implemented in a straightforward way in an MD routine, as all relevant pair distances are computed during the evaluation of energies and forces. The existing implementation stores all acceptor−hydrogen pairs, whenever the pair distance falls below a preset cutoff. In this study, the cutoff distance was 1.4 Å. This value ensures that only those hydrogens are considered which already show an increased separation from their donor atom. After propagation of all particles (MD simulations, geometry optimization) or the acceptance of the configuration (Monte Carlo simulations), the ratios $\rho$ of the stored acceptor−hydrogen pairs are evaluated at the new positions, and a topology update is performed if the respective ratio exceeds the threshold $\bar{\rho}$.

An adequate value of $\bar{\rho}$ has to be determined via observation of proton transfer events in actual simulation studies. The respective simulation protocol and findings are discussed in detail in the following sections.

**2.3. Simulation Protocol.** In order to identify a suitable value of $\bar{\rho}$ for the Garofalini model, the properties of proton transfer reactions were investigated by performing classical MD simulations. Although it is widely accepted that tunneling contributions are always important for the description of proton transfer reactions, it was shown by Parrinello et al. that the influence of tunneling strongly depends on the nature of the proton transfer.[46,47] While tunneling was found to be important in the case of the proton hole[46,47] (*e.g.*, between water and hydroxide), the barrier of a transfer involving an excess proton (*e.g.*, between water and oxonium) is low, and therefore, *"tunneling is negligible."*[47] It was concluded *"that* $H_5O_2^+$ *behaves in an essentially classical manner at 300 K."*[46] A similar finding was reported by Sagnella and Tuckerman based on a classical and path-integral MD study of $H_5O_2^+$ in the gas phase and aqueous solution employing an EVB approach: *"the quantum nature of the proton does not play a significant role in the proton transfer dynamics."*.[31] These findings have been discussed in further detail in the review articles of Marx[43] and Wraight.[48] For this reason, only acidified systems, namely an excess proton in water and 1 M HCl, were considered in this study.

The systems were composed of 1000 water molecules plus a single proton and 17 HCl molecules plus 1000 water molecules in cubic, periodic simulation boxes. The latter case corresponds to a 1 M HCl solution (3.59 wt %). The atomic interactions have been treated with the Garofalini model,[39,44] and the Velocity-Verlet algorithm[49,50] was employed to integrate the equations of motion with a time step of 0.2 fs. Following the parametrization of the model,[39,44] a Coulombic cutoff distance of 10.0 Å was set, and the long-range behavior of the Coulombic interaction was treated with the Wolf-summation method[41,42] with a damping coefficient of 0.224 $Å^{-1}$.[39,44] The systems were treated in the isobaric−isothermal ensemble (NpT) employing the Berendsen weak coupling algorithms[51] for thermostatization and pressurization. The target pressure was set to 1 atm; the temperatures chosen have been 283, 298, and 323 K for the system carrying an excess proton in water and 298 K in the case of 1 M HCl. All simulations have been equilibrated for 50 ps; the sampling time was 300 ps. Simulation data were stored every 5 fs.

As a final example, the application of the dissociative model in a hybrid QM/MM simulation using the quantum mechanical charge field ansatz[19,20] was demonstrated by investigating the hydrolytic conversion of As(III) to arsenous acid $H_3AsO_3$ in water. Aside from the employed water model,[39] the simulation protocol has been chosen identically to a previous investigation.[23]

The classical as well as QM/MM simulations have been performed with an implementation realized in the department. All quantum chemical computations in the MD simulations have been performed using the Turbomole program;[52−55] geometry optimizations have been performed using the Gaussian 09 package.[56]

**2.4. Analysis of Proton Diffusion.** A property of particular interest is the diffusion of protons in water. Wraight conjectured[48] that the proton diffusion can be split into two components: While the excess proton is bound to a $H_3O^+$, the diffusive properties are governed by the heavy oxygen atom. Due to the similar size of oxonium and $Na^+$, Wraight considered the diffusion coefficient of the sodium ion being


dx.doi.org/10.1021/ct300062k | J. Chem. Theory Comput. 2012, 8, 3586−3595

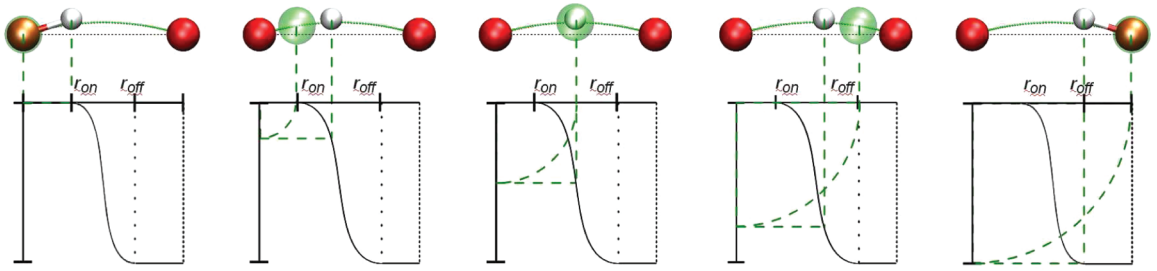


**Figure 3.** A locator particle (green sphere) is used to smoothly connect the donor and acceptor atoms as the hydrogen is transferred. The path is obtained via a constrained least-square fit to the donor-hydrogen and hydrogen-acceptor distance vectors. The position of the locator particle is determined via a smoothing function. To eliminate the influence of bond vibrations, the smoothing is only applied in the interval between $r_{on}$ and $r_{off}$.

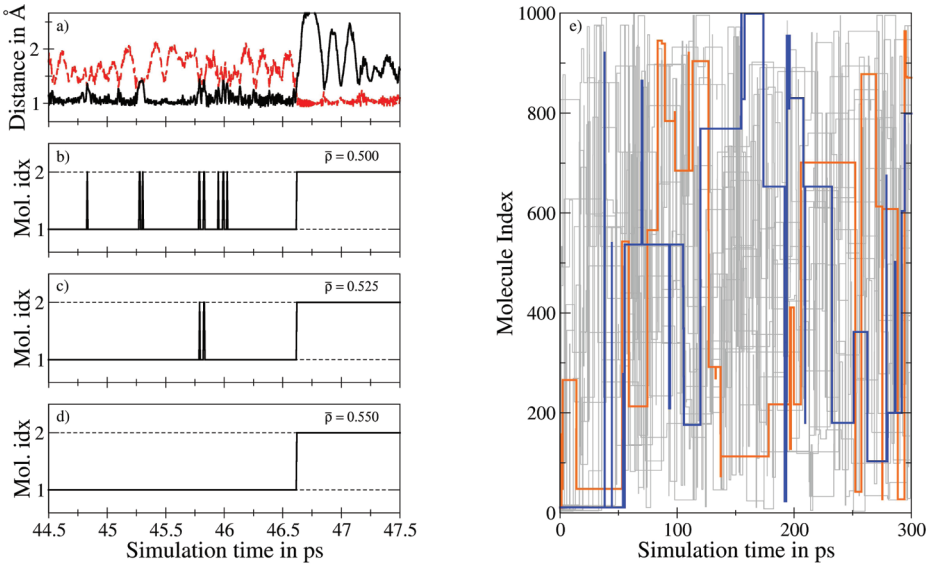


**Figure 4.** (a) Donor−hydrogen (black, solid line) and hydrogen−acceptor (red, dashed line) distances for an exemplary proton transfer event. (b−d) Influence of different ratios $\bar{p}$ on the topology update. (e) Proton transfer map showing the index of protonated water molecules for all 17 protons resulting from the simulation of 1 M HCl (two arbitrary plots are highlighted). Vertical lines represent registered exchange events and connect the participating water molecules.

$D_{Na^+}$ = 0.13 Å$^2$ ps$^{-1}$ for $H_3O^+$. Each proton transfer event leads to an increase of the diffusion until a new oxonium is formed. On the basis of the average lifetime of a proton transfer determined via NMR measurements as 1.33 ps[57] and the average O−O distance of 2.55 Å, Wraight estimated the diffusion coefficient for this step as $D_{H^+}$ = 0.81 Å$^2$ ps$^{-1}$. The sum of these values leads to *"good, but perhaps fortuitous, agreement"*[48] with the experimental value of 0.93 Å$^2$ ps$^{-1}$.[58,59]

The idea of combining both contributions does not consider the migration of a single proton throughout the solvent but is a measure of the diffusion of the associated excess charge by linking subsequent proton transfer events to a single diffusive entity. This approach is similar to the monitoring of the center of excess charge used in simulations employing empirical valence bond models,[32−36] in which the center of excess charge can be directly obtained via the results of the EVB subsystem.

Following the intuitive discussion of Wraight,[48] an analysis scheme should account for both components of the diffusion. As long as the donor-hydrogen bond is vibrating about its equilibrium position, the heavy donor atom governs the diffusion. Upon transfer of the proton, a smooth connection between the donor and acceptor atom should be established, so that at the end of the proton transfer the coordinate of interest resides at the acceptor atom.

The use of a locator particle (green sphere in Figure 3) that smoothly migrates from the donor to the acceptor atom is proposed. The path of this locator is determined via interpolation by performing a least-squares fit of a quadratic function to the donor-hydrogen and hydrogen-acceptor vectors with the constraint that the donor and acceptor positions act as end points in the fitting. This ensures a smooth connection of the donor and acceptor even if the hydrogen atom does not lie on the donor−acceptor vector (cf. Figure 3), while at the same time the distance traveled by the locator is not unnecessarily increased (which would be the case if a square function is fitted to the coordinates of the acceptor, donor, and hydrogen atoms, respectively).

The position of the locator particle is determined via a smoothing function employing the projected donor-hydrogen distance $r_{DH}^{\parallel}$ as a variable. The functional form of the smoothing function is given by the polynomial:

$$S(r) = 6(x - 0.5)^5 - 5(x - 0.5)^3 + \frac{15}{8}(x - 0.5) + 0.5 \quad (12)$$


dx.doi.org/10.1021/ct300062k | J. Chem. Theory Comput. 2012, 8, 3586−3595

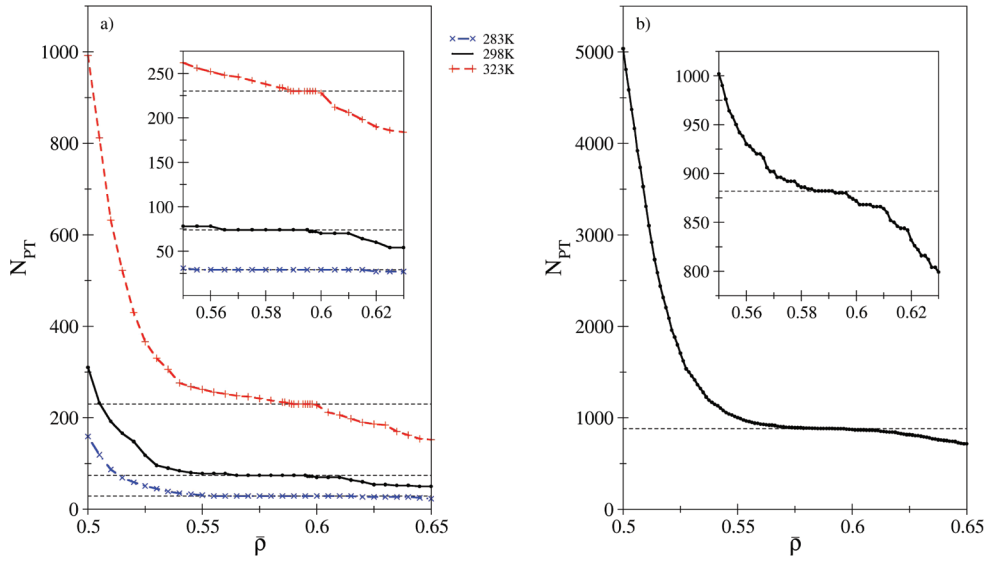


**Figure 5.** Number of registered proton transfer events $N_{PT}$ as a function of the ratio $\bar{\rho}$ resulting from MD simulations of (a) an excess proton in water and (b) 1 M HCl.

To avoid short-time fluctuations resulting from the vibration of the donor-hydrogen bonds, the smoothing is only applied in the interval $r_{on}$ and $r_{off}$ (cf. Figure 3), with $r_{off}$ being

$$r_{off} = r_{DA} - r_{on} \tag{13}$$

The optimal value of $r_{on}$ has to be determined by experimentation, but a value of about 1 Å appears to be reasonable. Thus, no displacement of the locator from the donor position occurs as long as the hydrogen is bound and a continuous migration of the locator from the donor to the acceptor particle is achieved upon proton transfer.

This interpolation scheme can be directly implemented in an analysis program for the diffusion coefficient $D$ using the Einstein relation

$$D = \frac{1}{2d} \lim_{t\to\infty} \frac{\langle(\mathbf{r}_t - \mathbf{r}_0)^2\rangle}{t} \tag{14}$$

where $\mathbf{r}_t$ and $\mathbf{r}_0$ correspond to the locator positions at time $t$ and the time origin, respectively, and $d$ is the dimensionality of the system.

In addition to the trajectory, the time-dependent topology is required as input, so that the exchanging proton and the respective donor and acceptor atoms are known. The interpolation yielding the coordinates of the locator particle can be performed while the analysis is executed. Visualization of the trajectory resulting for the locator particle overlaid with the original trajectory enables a lucid and intuitive depiction to monitor the interpolation.

In this work, a running evaluation window of 20 ps was used to compute the mean-square displacement, employing the last 5 ps for the regression to determine the diffusion coefficient.

## 3. RESULTS AND DISCUSSION

**3.1. Optimization of the Threshold Ratio $\bar{\rho}$.** To identify suitable settings of $\bar{\rho}$ registering only sustained proton transfer events, two systems have been investigated, namely an excess proton in 1000 waters and a 1 M HCl solution. In the first step, these systems have been simulated without applying any topology updates. Although the molecules rapidly become fragmented along the simulation, the underlying potential energy surface remained continuous. Afterwards, the topology update criterion was applied in a postprocessing step, yielding the number of proton transfer events as a function of simulation time as well as the time-dependent topology. The latter can be depicted in the form of proton transfer maps (PTM), by plotting the molecular indices of protonated water molecules as a function of the simulation time (see Figure 4b–e). Vertical lines represent registered exchange events and connect the participating water molecules.

As this investigation was carried out after the simulations were completed, the analysis was performed using different values for $\bar{\rho}$. The lower limit for $\bar{\rho}$ was chosen as 0.5, implying that the hydrogen has to be at least halfway between the donor and acceptor to be considered as exchanged. To estimate an upper limit, the properties of a standard hydrogen bond have been considered. Figure 2b depicts the minimum configuration of a water dimer optimized in implicit water[60,61] at the CCSD/cc-pVTZ[62] level. In this configuration, the acceptor–hydrogen ratio was found as 0.662, which acted as an upper limit for the analysis.

Figure 4a depicts the donor-hydrogen and hydrogen-acceptor distance for a selected proton transfer event. If a threshold ratio of 0.5 is employed, each fluctuation is registered as proton exchange, resulting in 17 topology updates (Figure 4b). An increase of $\bar{\rho}$ to 0.525 eliminates most of the short-time fluctuations, and only five topology updates are carried out (Figure 4c). After an increase of $\bar{\rho}$ to 0.55, only the sustained proton transfer event is registered (Figure 4d).

Figure 5a depicts the number of registered proton transfer events $N_{PT}$ as a function of the threshold ratio $\bar{\rho}$ resulting from three 300 ps MD simulations of an excess proton in water at different temperatures. In all cases, $N_{PT}$ shows a strong decrease at lower $\bar{\rho}$ values and reaches a plateau in the range of 0.55–0.6, indicating that only lasting proton transfer events are registered at this ratio, consistent with the example given in Figure 4a–d. A similar finding resulted from the 300 ps MD simulation of 1 M HCl (Figure 5b), although the plateau is narrower and shifted to larger $\bar{\rho}$ values (0.58–0.6). The centers of the respective plateaus suggest that a $\bar{\rho}$-setting ranging from 0.57 to 0.59 is a suitable choice for the threshold value, implying that


dx.doi.org/10.1021/ct300062k | J. Chem. Theory Comput. 2012, 8, 3586–3595

each proton has to travel until the projected donor-hydrogen bond length amounts to 57% to 59% of the donor−acceptor distance. This ensures that only lasting proton transfer events lead to a topology update, which is a crucial prerequisite for the application of the dissociative model in QM/MM simulations.

The time-dependent topology resulting for 1 M HCl using a ratio of 0.58 is shown in Figure 4e. The molecular indices of the protonated water molecules are depicted as a function of time. Similar to that in Figure 4b−d, each vertical line corresponds to a registered exchange event and connects those water molecules participating in the respective proton transfer reaction.

Choosing a ratio threshold of 0.59, the numbers of registered proton transfer events are 29, 74, and 230 in the case of the 300 ps MD simulations of an excess proton in water at 283, 298, and 323 K, respectively. In the case of 1 M HCl at 298 K, a total of 882 exchanges have been observed within 300 ps, which amounts to 48.4 transfer events per proton. The corresponding proton hopping rates $h$ given as the quotient of the number of exchanges and the simulation time are listed in Table 1. The

**Table 1. Comparison of the Proton Hopping Rate $h$ in ps$^{-1}$ Resulting from Different Approaches**

| | | |
|---|---|---|
| Excess Proton | | |
| Garofalini 283 K | 0.10 | this work |
| Garofalini 298 K | 0.25 | this work |
| Garofalini 323 K | 0.77 | this work |
| MS-EVB2 298 K | 0.16 | 36 |
| MS-EVB3 298 K | 0.16 | 36 |
| MS-EVB 298 K | 0.25 | 32 |
| CPMD 298 K | 0.5 | 67 |
| experimental | 0.75 | 57 |
| 1 M HCl | | |
| Garofalini 298 K | 0.17 | this work |

hopping rate obtained for the excess proton at 298 K of 0.25 ps$^{-1}$ is within the estimated range resulting from EVB and CPMD approaches. The value of 0.75 ps$^{-1}$ is derived from the experimentally determined (NMR) mean residence time of an excess proton[57] being approximately 1.33 ps.[48] The deviation between the data obtained via simulations and the experimental value can be explained via contributions of nuclear quantum effects. Although it was shown that tunneling contributions are negligible in transfer reactions of excess protons,[31,46,47] zero-point vibrations resulting also from nuclear quantum effects may lower the barrier in the reaction coordinate,[43] which would promote proton transfer events.

A proton hopping rate of 0.17 ps$^{-1}$ was determined for 1 M HCl at 298 K, which is lower than the value obtained for the excess proton. Considering the large number of solvated species and the associated increase of the electrostatic character within the solution, a reduction of the proton hopping rate was to be expected.

**3.2. Evaluation of the Diffusion Constant of the Center of Excess Charge.** The obtained topology data can be used to compute the diffusion of the excess charge by employing a locator particle to smoothly connect the donor and acceptor atoms of the respective molecules as outlined in the Methodology section. To avoid a corruption of the interpolation resulting from intramolecular vibrations of the donor-hydrogen bonds when calculating the mean-square displacement, the smoothing is only applied within the threshold distances $r_{on}$ and $r_{off}$ (cf. Figure 3).

Figure 6 shows the dependence of the diffusion coefficient $D$ as a function of $r_{on}$, employing different ratios $\bar{\rho}$ in the topology update. As expected, $D$ is almost unaffected for $r_{on}$ values larger than 1 Å, whereas slopes are observed at decreasing $r_{on}$, as the vibrational amplitudes of the donor-hydrogen bonds overlap with the smoothing region. By setting $r_{on}$ too large (approximately 1.3 Å), the smoothing function is effectively turned off, and the interpolation turns into a step function (not shown). Thus, the recommended setting for $r_{on}$ lies between 1.0 and 1.3 Å, in which the diffusion coefficient is almost not influenced by the choice of $r_{on}$ and the ratio $\bar{\rho}$. The respective deviations in $D$ are on the fourth significant digit.

Table 2 lists the diffusion coefficient for the center of excess charge resulting from the MD simulations of a single excess proton in water resulting from various approaches and 1 M HCl. The value of $D$ lies well within the range estimated by the different EVB approaches in the case of the excess proton in water at 298 K. In order to investigate the influence of the temperature and pressure coupling on the diffusive properties, simulations in the NVE ensemble at the average densities obtained from the NpT runs have been performed for 500 000 MD steps (100 ps) of sampling. As the influence of temperature and density variations average over time in the NpT case, NVE simulations performed close to the average densities and temperatures of the NpT runs are expected to yield similar values for the diffusion coefficient. The average

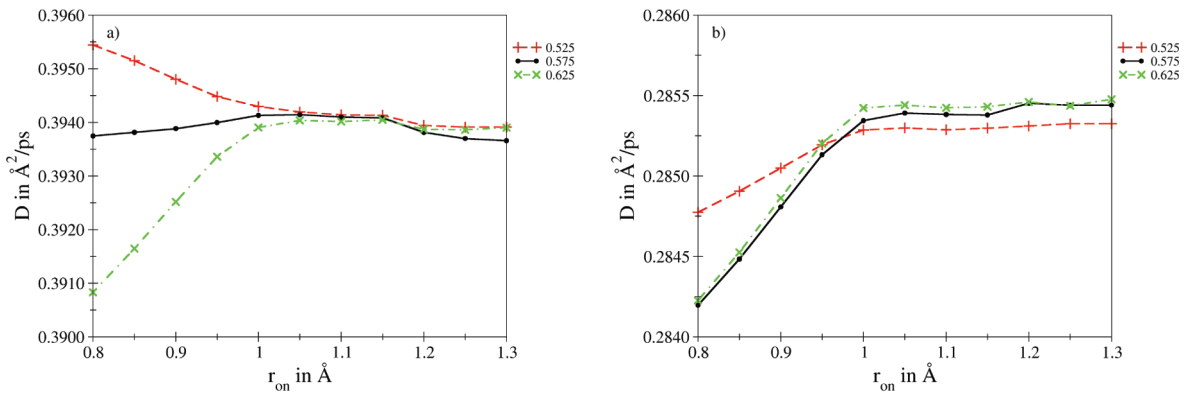


**Figure 6.** Diffusion coefficient $D$ as a function of $r_{on}$ for different values of $\bar{\rho}$ (0.525, 0.575, 0.625) obtained from MD simulations of (a) an excess proton in water at 298 K and (b) 1 M HCl.

**Table 2. Comparison of the Diffusion Coefficient $D$ in Å$^2$/ps of the Center of Excess Charge Resulting from Different Approaches**

| | | |
|---|---|---|
| Excess Proton | | |
| Garofalini 283 K (NpT) | 0.25 | this work |
| Garofalini 283 K (NVE) | 0.26 | this work |
| Garofalini 296 K (NpT) | 0.39 | this work |
| Garofalini 298 K (NVE) | 0.38 | this work |
| Garofalini 323 K (NpT) | 0.61 | this work |
| Garofalini 325 K (NVE) | 0.67 | this work |
| MS-EVB2 298K | 0.29 | 36 |
| MS-EVB 298K | 0.35 | 34 |
| MS-EVB3 298K | 0.36 | 36 |
| aMS-EVB3 298K | 0.41 | 37 |
| qMS-EVB3 298K | 0.50 | 36 |
| MS-EVB 298K | 0.77 | 33 |
| MS-EVB 298K | 0.83 | 35 |
| experimental | 0.93 | 58, 59 |
| 1 M HCl | | |
| Garofalini 298 K (NpT) | 0.29 | this work |

temperatures for the three NVE runs are 282.6, 296.1, and 324.6 K. The corresponding diffusion coefficients are 0.26, 0.38, and 0.67 Å$^2$/ps, which agree well with the NpT values found as 0.25, 0.38, and 0.61 Å$^2$/ps at 283, 298, and 323 K and 1 atm, respectively. The largest deviations have been observed in the case of the highest temperature, whereas the diffusion coefficients are almost not influenced at the lower temperatures. The drifts of the total energy in the NVE obtained from linear regression amount to $5.1 \times 10^{-5}$, $9.9 \times 10^{-5}$, and $1.8 \times 10^{-4}$ kcal/mol ps. Over the course of a 100 ps trajectory, this corresponds to drifts of $2.9 \times 10^{-6}$, $5.7 \times 10^{-6}$, and $1.0 \times 10^{-5}$% of the total energy. These numbers imply that the chosen time step of 0.2 fs results in an appropriate conversion of the total energy.

The deviation between the experimental value and the theoretical estimations can be explained by a lowering of the activation barrier resulting from zero point vibration[43] as discussed in the previous section. An EVB study estimated that the inclusion of nuclear quantum effects leads just to a moderate increase of the diffusion coefficient by a factor of 1.7.[36] Nevertheless, the application of simulation strategies accounting for these effects[28,63−66] is envisaged for the future, to investigate their influence on the performance of the Garofalini model.[39]

In the case of the 1 M HCl simulation, a lowered diffusion coefficient 0.29 Å$^2$/ps was observed. Similar to the case of the proton hopping rate, the large number ions and the increased electrostatic background were expected to reduce the diffusive properties of the individual species within solution.

**3.3. Application in a Hybrid QM/MM Simulation.** This section presents an application of the dissociative potential in a hybrid QM/MM simulation. A previous investigation[23] of the hydrolytic conversion of As(III) to arsenous acid $H_3AsO_3$ via

$$As^{3+} + 3H_2O \leftrightharpoons H_3AsO_3 + 3H^+ \quad (15)$$

suffered from the inability of conventional water potentials to describe the (de)protonation of water molecules. Two of the three possible proton transfer events, each creating an oxonium−hydroxide pair, were observed within the simulation time. As long as the respective species remained within the quantum chemically treated region, the simulation did not encounter any obstacles. However, while the hydroxide ions remained bound to the arsen atom, the $H_3O^+$ ions were soon migrating from the QM to the MM zone. At this point, the transferred proton had to be deleted from the system, and a reassignment of the residue types was carried out to continue the simulation. This intervention resulted in a disconnected trajectory requiring a further equilibration of the system to adjust to the discontinuous modification of the system.

This situation does not arise if the dissociative force field is employed to model the solvent in the MM region. As the

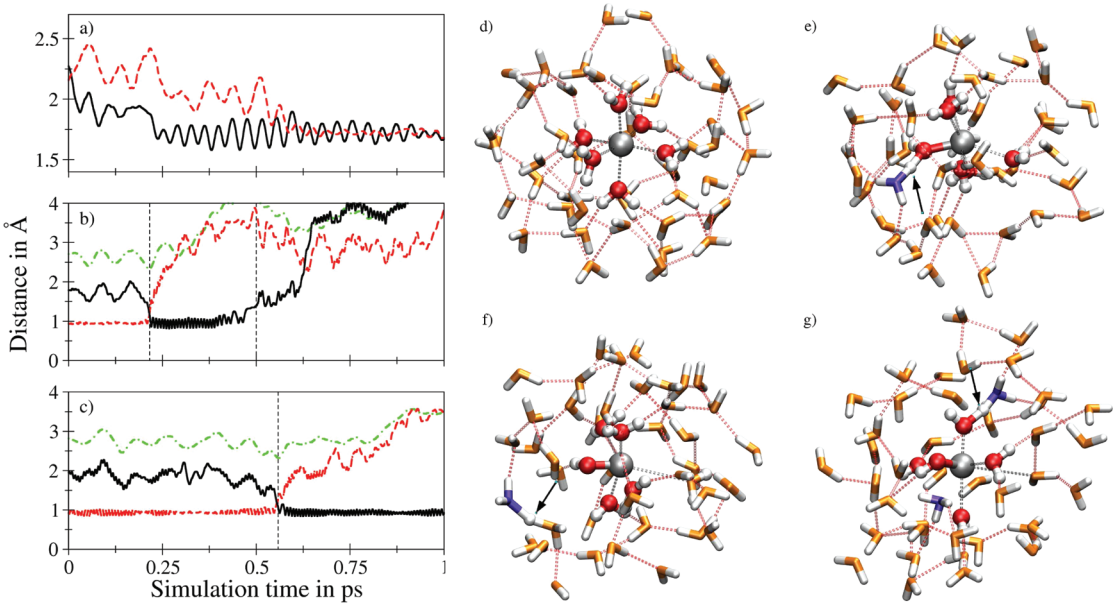


**Figure 7.** (a) As−O and (b,c) hydrogen-acceptor (solid black line), donor-hydrogen (red dashed line), and donor-acceptor (green dash-dotted line) distances for the proton transfer events occurring in the first picosecond. (d) Initial configuration. (e) First proton transfer event induced by As(III) (0.21 ps) (f) Another proton transfer of the newly formed $H_3O^+$ (0.5 ps). (g) Second proton transfer event induced by $[As(OH)]^{2+}$ (0.56 ps).


dx.doi.org/10.1021/ct300062k | J. Chem. Theory Comput. 2012, 8, 3586−3595

implementation of the automated topology update provides information on the composition of all residues at each step of the simulation, solvent molecules and their (de)protonated counterparts can be assigned as a whole to either the QM or the MM regions. Oxonium and hydroxide species may migrate freely from the QM to the MM region and vice versa. No manual intervention was required to reassign residue types, and despite the discontinuity of the topology updates, the underlying potential energy surface remained continuous.

In this work, two of the three possible hydrolysis events were registered within the first picosecond of the simulation. Figure 7a–c depicts the time series of the associated As–O as well as the donor-hydrogen, hydrogen-acceptor, and donor-acceptor distances. After 0.21 ps, the first proton transfer event took place—a water molecule coordinated to the As(III) was deprotonated, and a $[As(OH)]^{2+}$ complex was formed (Figure 7e). After a short time, another hydrogen migrated from the newly formed oxonium ion to a water molecule in the bulk at a simulation time of 0.5 ps (Figure 7f). At 0.56 ps, the second hydrolysis event was induced by $[As(OH)]^{2+}$, forming a $[As(OH)_2]^{+}$ complex (Figure 7f). Similarly, the transferred proton was migrating toward the bulk via a number of proton transfer reactions.

Although the first two steps of the hydrolysis took place within the first picosecond of the simulation, the third stage which would finally lead to arseneous acid $H_3AsO_3$ was not observed within the 20 ps trajectory. As the charge on the complex is reduced by the two hydroxide ions, the probability for this reaction to occur is much lower than for the first two hydrolysis processes. Nevertheless, a number of attempted proton transfer events of first shell water molecules have been observed, indicating that this process is likely to occur if the simulation time is increased.

## 4. CONCLUDING REMARKS

This work presents an implementation strategy for a dissociative solvent potential in hybrid QM/MM simulations. A crucial prerequisite is the availability of molecular topology data at every step of the simulation, to avoid a fragmentation of the solvent molecules, which would render the execution of such simulations unfeasible. This topology information can be obtained by monitoring all occurring proton transfer events as the simulation is progressing. This was achieved by introducing a simple and effective update condition based on the ratio of the projected donor-hydrogen bond length and the donor-acceptor distance. Evaluation of the number of proton transfer events from classical MD simulations enabled the determination of an optimal setting for the threshold ratio $\bar{\rho}$ being in the range of 0.58–0.60, ensuring that only sustained proton transfer events trigger a topology update. While this time-dependent topology is essential for the execution of QM/MM studies, other simulation approaches such as classical or Car–Parrinello MD simulations can benefit from this approach as well. The resulting topology data can be directly employed in post-processing analysis such as the determination of the proton hopping rate $h$ and the diffusion coefficient $D$.

For the latter, an evaluation strategy employing an interpolation scheme following the center of excess charge with the help of a locator particle has been presented. The approach follows the concept that $D$ is limited by the diffusion of the oxonium ion, interrupted by occasionally occurring proton transfer events, which lead to an increase in $D$. Although the diffusion coefficient and the proton hopping rate determined for the Garofalini model are lower than the experimental determination, the values are well within the range estimated from EVB and CPMD approaches. To investigate the influence of zero-point vibrational contributions on the proton transfer dynamics, simulations employing path-integral approaches are envisaged for the future. Both the topology update criterion and the interpolation scheme for the determination of the diffusion coefficient can be directly applied to this kind of simulation.

The implementation of the dissociative model in a QM/MM MD simulation was demonstrated by investigating the hydrolytic conversion of As(III) to $H_3AsO_3$ in aqueous solution. Although the simulation time of 20 ps was too short to observe the third stage of the hydrolysis, the formation of the $[As(OH)_2]^{+}$ species and the subsequent migration of the newly formed oxonium ions into the MM region demonstrate the capabilities of this simulation protocol. The capability of the MM potential to describe (de)protonated solvent molecules enables the continuation of the simulation whenever such a species migrates from the QM to MM region. On the other hand, the general applicability of the quantum chemical treatment enables investigations of proton transfer phenomena also in those cases, where no adequate solute–solvent potentials are available. As parameters for $Na^{+}$ and $Cl^{-}$ ions have been developed for the Garofalini model as well, this approach can also be used to model solutions at different pH values, which can be employed to induce chemical reactions of solutes located in the quantum mechanical zone.

Although the execution of hybrid QM/MM simulations is significantly more demanding than classical simulations, a combination of the ansatz presented in this manuscript with path-integral approaches appears to be a promising long-term goal. The resulting methodology will enable the study of nuclear quantum effects combined with a quantum chemical description of the electronic potential energy surface, while at the same time a sufficiently large system size mandatory for the modeling of acidified and basic solutions can be retained.

## AUTHOR INFORMATION

### Corresponding Author

*Tel.: +43-512-507-57102. Fax: +43-512-507-57199. E-mail: T.Hofer@uibk.ac.at.

### Notes

The authors declare no competing financial interest.

## ACKNOWLEDGMENTS

Financial support by the Austrian Science Fund (FWF) is gratefully acknowledged (Project J 2833).

## DEDICATION

Dedicated to Prof. Dr. Wilfred F. van Gunsteren on the occasion of his 65th birthday.

## REFERENCES

(1) Allen, M. P.; Tildesley, D. J. *Computer Simulation of Liquids*; Oxford Science Publications: Oxford, U.K., 1990.

(2) Sadus, R. J. *Molecular Simulation of Fluids: Theory, Algorithms, and Object-Orientation*; Elsevier: Amsterdam, 1999.

(3) Hünenberger, P.; Reif, M. *Single Ion Solvation*; RSC Publishing: Cambridge, U.K., 2011.

(4) Leach, A. R. *Molecular Modelling*, 2nd ed.; Prentice-Hall: Harlow, England, 2001.

(5) Jensen, F. *Introduction to Computational Chemistry*, 2nd ed.; John Wiley & Sons Ltd.: Chichester, U. K., 2006.
(6) Szabo, A.; Ostlund, N. S. *Modern Quantum Chemistry*; Dover Publications: New York, 1996.
(7) Helgaker, T.; Jørgensen, P.; Olsen, J. *Molecular Electronic Structure Theory*; Wiley: Chichester, U. K., 2000.
(8) Koch, W.; Holthausen, M. C. *A Chemist's Guide to Density Functional Theory*, 2nd ed.; Wiley−VCH: Weinheim, Germany, 2002.
(9) Schrödinger, E. *Ann. Phys* **1926**, *81*, 109.
(10) Car, R.; Parrinello, M. *Phys. Rev. Lett.* **1985**, *55* (22), 2471.
(11) Yoo, S.; Zeng, X. C.; Xantheas, S. *J. Chem. Phys.* **2009**, *130*, 221102.
(12) Schmidt, J.; VandeVondele, J.; Kuo, I.; Sebastiani, D.; Siepmann, J.; Hutter, J.; Mundy, C. J. *J. Phys. Chem. B* **2009**, *113*, 11959−11964.
(13) Senn, H. M.; Thiel, W. *Curr. Opin. Chem. Biol.* **2007**, *11*, 182.
(14) Lin, H.; Truhlar, D. G. *Theor. Chim. Acta* **2007**, *117*, 185.
(15) Warshel, A.; Levitt, M. *J. Mol. Biol.* **1976**, *103*, 227.
(16) Field, M. J.; Bash, P. A.; Karplus, M. *J. Comput. Chem.* **1990**, *11* (6), 700.
(17) Gao, J. *J. Am. Chem. Soc.* **1993**, *115*, 2930.
(18) Bakowies, D.; Thiel, W. *J. Phys. Chem.* **1996**, *100* (25), 10580.
(19) Rode, B. M.; Hofer, T. S.; Randolf, B. R.; Schwenk, C. F.; Xenides, D.; Vchirawongkwin, V. *Theor. Chem. Acc.* **2006**, *115*, 77.
(20) Hofer, T. S.; Pribil, A. B.; Randolf, B. R.; Rode, B. M. *Adv. Quantum Chem.* **2010**, *59*, 213.
(21) Heyden, A.; Lin, H.; Truhlar, D. G. *J. Phys. Chem. B* **2007**, *111*, 2231.
(22) Bulo, R. E.; Ensing, B.; Sikkema, J.; Visscher, L. *J. Chem. Theory Comput.* **2009**, *5* (9), 2212.
(23) Bhattacharjee, A.; Hofer, T. S.; Pribil, A. B.; Randolf, B. R.; Rode, B. M. *Chem. Phys. Lett.* **2009**, *473*, 176.
(24) Bhattacharjee, A.; Hofer, T. S.; Pribil, A. B.; Randolf, B. R.; Rode, B. M. *Phys. Chem. Chem. Phys.* **2010**, *12*, 6244.
(25) Stillinger, F. H.; Rahman, A. *J. Chem. Phys.* **1978**, *68*, 666.
(26) Rahman, A.; Stillinger, F. H.; Lemberg, H. L. *J. Chem. Phys.* **1975**, *63*, 5223.
(27) Stillinger, F. H. *Adv. Chem. Phys.* **1975**, *31*, 1.
(28) Billeter, S. R.; van Gunsteren, W. F. *Comput. Phys. Commun.* **1997**, *107*, 61.
(29) Billeter, S. R.; van Gunsteren, W. F. *J. Phys. Chem. A* **1998**, *102*, 4669.
(30) Warshel, A.; Weiss, R. M. *J. Am. Chem. Soc.* **1980**, *102*, 6218.
(31) Sagnella, D. E.; Tuckerman, M. E. *J. Chem. Phys.* **1998**, *108*, 2072.
(32) Schmitt, U. W.; Voth, G. A. *J. Phys. Chem. B* **1998**, *102*, 5547.
(33) Vuilleumier, R.; Borgis, D. *J. Chem. Phys.* **1999**, *111*, 4251.
(34) Čuma, M.; Schmitt, U. W.; Voth, G. A. *J. Phys. Chem. A* **2001**, *105*, 2814.
(35) Brancato, G.; Tuckerman, M. E. *J. Chem. Phys.* **2005**, *122*, 224507.
(36) Wu, Y.; Chen, H.; Wang, F.; Paesani, F.; Voth, G. A. *J. Phys. Chem. B* **2008**, *112*, 467.
(37) Park, K.; Lin, W.; Paesani, F. *J. Phys. Chem. B* **2012**, *116*, 343.
(38) Ufimtsev, I. S.; Kalinichev, A. G.; Todd, M. J.; Kirkpatrick, R. J. *Phys. Chem. Chem. Phys.* **2009**, *11*, 9420.
(39) Mahadevan, T. S.; Garofalini, S. H. *J. Phys. Chem. B* **2007**, *111*, 8919.
(40) Guillot, B. *J. Mol. Liq.* **2002**, *101*, 219.
(41) Wolf, D.; Keblinski, P.; Phillpot, S. R.; Eggebrecht, J. *J. Chem. Phys.* **1999**, *110*, 8254.
(42) Fennell, C. J.; Gezelter, J. D. *J. Chem. Phys.* **2006**, *124*, 234104.
(43) Marx, D. *ChemPhysChem* **2006**, *7*, 1848.
(44) Webb, M. B.; Garofalini, S. H.; Scherer, G. W. *J. Phys. Chem. B* **2009**, *113*, 9886.
(45) Li, X.; Walker, B.; Michaelides, A. *Proc. Natl. Acad. Sci. U.S.A.* **2011**, *108*, 6369.
(46) Tuckerman, M.; Marx, D.; Klein, M.; Parrinello, M. *Science* **1997**, *275*, 817.
(47) Marx, D.; Tuckerman, M. E.; Hutter, J.; Parrinello, M. *Nature* **1999**, *397*, 601.
(48) Wraight, C. A. *Biochim. Biophys. Acta* **2006**, *1757*, 886.
(49) Verlet, L. *Phys. Rev.* **1967**, *159*, 98.
(50) Swope, W. C.; Andersen, H. C.; Berens, P. H.; Wilson, K. R. *J. Chem. Phys.* **1982**, *76*, 637.
(51) Berendsen, H. J. C.; Postma, J. P. M; van Gunsteren, W. F.; DiNola, A.; Haak, J. R. *J. Phys. Chem.* **1984**, *81*, 3684−3690.
(52) Ahlrichs, R.; Bär, M.; Häser, M.; Horn, H.; Kölmel, C. *Chem. Phys. Lett.* **1989**, *162*, 165−169.
(53) Brode, S.; Horn, H.; Ehrig, M.; Moldrup, D.; Rice, J. E.; Ahlrichs, R. *J. Comput. Chem.* **1993**, *14*, 1142−1148.
(54) Ahlrichs, R.; von Arnim, M. In *Methods and Techniques in Computational Chemistry: METECC-95*; Clementi, E., Corongiu, G., Eds.; STEF: Cagliari, Italy, 1995; Chapter 13, pp 509−554.
(55) von Arnim, M.; Ahlrichs, R. *J. Comput. Chem.* **1998**, *19*, 1746−1757.
(56) Frisch, M. J.; Trucks, G. W.; Schlegel, H. B.; Scuseria, G. E.; Robb, M. A.; Cheeseman, J. R.; Scalmani, G.; Barone, V.; Mennucci, B.; Petersson, G. A.; Nakatsuji, H.; Caricato, M.; Li, X.; Hratchian, H. P.; Izmaylov, A. F.; Bloino, J.; Zheng, G.; Sonnenberg, J. L.; Hada, M.; Ehara, M.; Toyota, K.; Fukuda, R.; Hasegawa, J.; Ishida, M.; Nakajima, T.; Honda, Y.; Kitao, O.; Nakai, H.; Vreven, T.; Montgomery, J. A., Jr.; Peralta, J. E.; Ogliaro, F.; Bearpark, M.; Heyd, J. J.; Brothers, E.; Kudin, K. N.; Staroverov, V. N.; Kobayashi, R.; Normand, J.; Raghavachari, K.; Rendell, A.; Burant, J. C.; Iyengar, S. S.; Tomasi, J.; Cossi, M.; Rega, N.; Millam, J. M.; Klene, M.; Knox, J. E.; Cross, J. B.; Bakken, V.; Adamo, C.; Jaramillo, J.; Gomperts, R.; Stratmann, R. E.; Yazyev, O.; Austin, A. J.; Cammi, R.; Pomelli, C.; Ochterski, J. W.; Martin, R. L.; Morokuma, K.; Zakrzewski, V. G.; Voth, G. A.; Salvador, P.; Dannenberg, J. J.; Dapprich, S.; Daniels, A. D.; Foresman, J. B.; Ortiz, J. V.; Cioslowski, J.; Fox, D. J. *Gaussian 09*, Revision A.1; Gaussian Inc.: Wallingford, CT, 2009.
(57) Luz, Z.; Meiboom, S. *J. Am. Chem. Soc.* **1964**, *86*, 4768.
(58) Roberts, N. K.; Northey, H. L. *J. Chem. Soc., Faraday Trans.* **1974**, *70*, 253.
(59) Pines, E.; Huppert, D.; Agmon, N. *J. Chem. Phys.* **1988**, *88*, 5620.
(60) Cramer, C. J.; Truhlar, D. G. *Chem. Rev.* **1999**, *99*, 2161.
(61) Tomasi, J.; Mennucci, B.; Cammi, R. *Chem. Rev.* **2005**, *105*, 2999.
(62) Dunning, T. Jr. *J. Chem. Phys.* **1989**, *90*, 1007.
(63) Cao, J.; Voth, G. A. *J. Chem. Phys.* **1994**, *100*, 5093.
(64) Cao, J.; Voth, G. A. *J. Chem. Phys.* **1994**, *100*, 5106.
(65) Marx, D.; Parrinello, M. *J. Chem. Phys.* **1996**, *104*, 4077.
(66) Craig, I. R.; Manolopoulos, D. E. *J. Chem. Phys.* **2004**, *121*, 3368.
(67) Tuckerman, M.; Laasonen, K.; Sprik, M.; Parrinello, M. *J. Chem. Phys.* **1995**, *103*, 150.